

A facile pot synthesis of (Ti_3AlC_2) MAX phase and its derived MXene ($Ti_3C_2T_x$)

Pragya Dixit, Tanmoy Maiti*

Plasmonics and Perovskites Laboratory, Department of Materials Science and Engineering, IIT Kanpur, UP, 208016, India



ABSTRACT

Various processing techniques reported in the literature for synthesizing the Ti_3AlC_2 MAX phase involve high calcination temperature, expensive equipment, and inert environmental requirement. Here, we report a cost-effective, solid-state, single-step synthesis route of the Ti_3AlC_2 MAX phase. Optimizing the stoichiometry of the precursors and controlling the thermal treatment, the desired MAX phase has been attained, as confirmed by XRD analysis. Further, $Ti_3C_2T_x$ (where, T_x : O, OH, F functional groups) MXene was prepared from this one-pot synthesized MAX phase. FESEM, TEM, and Raman spectroscopy were used to ensure that the hexagonal structure of the MAX phase was retained in as-synthesized MXene. Further, XPS was employed to detect the presence of surface functional groups (-O, -OH, and -F) on the MXene surface. UV-vis spectroscopy shows a strong absorption peak in the NIR region.

1. Introduction

Since the discovery of new generation 2D material MXene, efforts towards developing a recipe of low-cost, easy processing technique for MAX as MXene precursor have been revived. This family of 2D materials is named MXene to recognize its parent ternary compound MAX and show the similarities with famous 2D materials like Graphene [1]. Their exotic properties such as high flexibility [2], layered structure to host ions and molecules [3], high young's modulus [4], and high electrical conductivity (24000 S cm^{-1}) [5] make them potential candidates for a wide range of applications, including catalysis [6], water desalination [7], gas sensor [8,9], electromagnetic interference shielding [10], super capacitor [11] and electrochemical energy storage [12,13]. Although MXene has already been established as a promising energy storage material in Li-ion (Na ion) batteries, it's yet to realize widespread industrial applications. Ease of synthesis can be an excellent way to make it viable for a variety of applications.

MAX is a ternary phase compound, where M is an early transition metal element (e.g., Sc, Ti, V, Cr), A is a group 14 or group 15 element (e.g., Al, Si, Ga), and X is C and N. Formula for MAX is $M_{n+1}AX_n$, where n lies between 1 and 3. Fig. 1(a) shows the typical crystal structure of M_3AX_2 , where M atoms are located at closely packed sites; X atoms occupy the octahedral sites. Every 4th layer consists of a group A element weakly bonded with M atoms. MAX shows a hexagonal structure with space group $P6_3/mmc$ and two formula units per cell. Many processing techniques have been explored to make MAX phases. However, the difficulty in synthesizing high purity phase either in bulk or

powder form has led researchers to explore multistep synthesis routes. Barsoum [14] prepared Mo_2Ga_2C by ball milling Mo_2C and Ga and two-step processing with a long dwelling time, introducing the impurity of MgO and some free Ga. Hu et al. [15] prepared Nb_4AlC_3 using a dispersing agent with milling media. The appropriate Nb, Al, and C molar ratio was ball milled and sintered by the SPS route at 1450°C . The sample was also kept in a magnetic field to orient the particles toward the magnetic field. Goto et al. [16] adopted the CVD (chemical vapor deposition) approach to synthesize the MAX phase. They used $TiCl_4$, $SiCl_4$, H_2 , and CCl_4 as source gases. Pampuch et al. [17] reported the formation of Ti_3SiC_2 by igniting the stoichiometric mixture of Ti, Si, and C at 1830°C . A porous product was formed with some fraction of $\sim 20\text{ wt\% TiC}$. Racault et al. [18] reported a multistep solid-state synthesis process to make Ti_3AlC_2 with $>5\text{ wt\% TiC}$. All these reports suggest that the synthesis history of the MAX phase, which is the key precursor for the synthesis of MXene, imparts its characteristics into 2D MXene [19–21], e.g., the presence of oxide in MAX will also reflect in structural and electrical properties of MXene. Therefore, it is imperative to explore a laboratory synthesis route of the high purity MAX phase. The production cost of the pure MAX phase has been relatively high [19,21,22], which further restricts its broad applicability. Hence, it is essential to find a single-step, cost-efficient way of synthesizing MAX phase. The current research work studies the effect of the right choice of precursors, sub-stoichiometric composition, and temperature on the final product phase. It indicates a narrow temperature window for the synthesis of Ti_3AlC_2 (312 MAX phase).

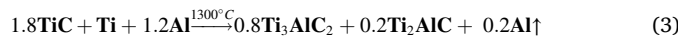
* Corresponding author.

E-mail address: tmaiti@iitk.ac.in (T. Maiti).

2. Experimental details

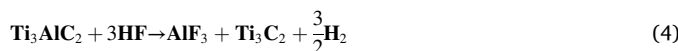
2.1. Synthesis of MAX phase

In the present work, commercial-grade TiC (>99%, Sigma Aldrich), Al (98%, Alfa Aesar), and Ti (99.5%, Alfa Aesar) were used as precursors. Precursors were weighed in the stoichiometric ratio. An excess amount of Al was taken to maintain the stoichiometry and cope with its high evaporation rate at a higher temperature. As shown in Fig. 1(b), weighed powder was hand-mixed using agate mortar and pestle, followed by cold compaction using a uniaxial hydraulic press. Compacted pellets were vacuum-sealed in a 10 cm long fused quartz tube and kept in a muffle furnace. The calcination temperature was varied from 1300 °C to 1350 °C with a soaking time of 1–2 h to get the desired MAX (Ti_3AlC_2) phase. It is to be noted that calcination at 1350 °C performed for 1 hr since the quartz ampoule started swelling just after 1 h of heat treatment and broke during 2 h of firing. Fig. 2(a) shows that sealing in a quartz tube is an effective way to avoid the oxidation of Ti and Al metals. Following reactions are expected to occur using a stoichiometric and sub-stoichiometric ratio of precursors.



2.2. Synthesis of MXene

1 gm of a lightly sintered pellet of Ti_3AlC_2 was finely crushed with agate mortar and pestle. This powder was mixed in the 20 ml, 48 wt% HF for 8 h to selectively etch Al and get a 2-D layered structure. Etching was done in high-density polyethylene (HDPE) crucible, placed on a magnetic stirrer hot plate at room temperature, as shown in Fig. 2. The Teflon-coated magnetic bead was used for continuous stirring while etching. Afterward, the solution was washed with DI water and centrifuged at 5000 rpm for 3 min s until pH > 6 was obtained. Water was decanted, and settled powder was removed from the centrifuge tube and kept for vacuum drying at 60 °C for 8 h s. The dried powder was much darker in color because of the removal of Al. This powder was used for further characterization.



Equations (4)–(6) and Fig. 3 show the mechanism of MXene (Ti_3C_x) formation and the presence of functional groups after etching with HF and washing the solution with DI water.

2.3. Characterization

XRD was performed on Rigaku MiniFlex 600, with a step size of 0.02° with Cu K α radiation (30 kV and 10 mA). For Surface characterization, elemental composition detection, and electronic and chemical states of the elements were determined using X-Ray Photoelectron Spectroscopy on PHI 5000Versa Prob II, FEI Inc. with Ar ion and C60 sputter gun. Raman spectroscopy was done on Princeton Instruments Acton Spectra Pro 2500i, with 532 nm DPSS Laser (Laser Quantum gem 50 MW). A 50X objective lens, a grating of 1200 lines per mm, was used to get high spectral resolution. Microstructural characterization was done using the FESEM Quanta200 instrument. The SAED pattern was observed using FEI-Tecnai G2 Tin TEM 120 kV for further structural verification. The four-probe van der Pauw method was used to check the thin samples' electrical conductivity. A Semiconductor Parameter analyzer measured I–V characteristics.

3. Results and discussion

3.1. XRD

XRD pattern of dense pellet fired at 1300 °C shown in Fig. 4 implies the formation of Ti_3AlC_2 (Reference pattern:00-052-0875) as the primary phase with Ti_2AlC (Reference pattern:00-029-0095) MAX phase and $TiC_{0.93}$ (Reference pattern:03-065-8806) as a by-product. A peak at $2\Theta = 9.6$ of (002) basal plane, which is the typical peak of Ti_3AlC_2 as reported by Barsoum and others [1,23], confirms the formation of desired MAX phase. Fig. 4(a) depicts that the peak at around $2\Theta = 39^\circ$ is completely diminished after etching, confirming Al atoms' removal from the 3D lattice. Fig. 4(b) shows a broad (002) peak for MXene, showing a significant shift from 9.5° to 8.29° , depicting the increased interlayer spacing of MXene flakes [1]. To reduce the TiC content in the MAX phase, we have increased the firing temperature to 1350 °C. Interestingly, an increase in MAX phase processing temperature results in a lower yield of the Ti_3AlC_2 MAX phase, as shown in Fig. 4(c). It is anticipated that the stoichiometric ratio of precursors (Ti: Al: TiC: 1:1:2) does not provide sufficient vacant sites for Al to go into the Ti_3AlC_2 MAX structure in the higher fraction of TiC in the finally obtained MAX phase. Hence, we have further adopted the strategy of using a sub-stoichiometric ratio of precursors (Ti:Al: TiC:1:1.2:1.8).

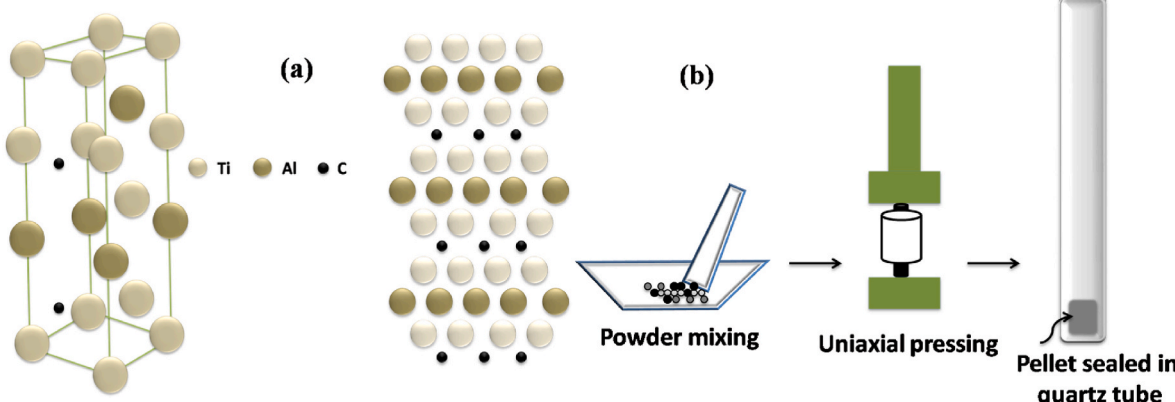


Fig. 1. (a) Schematic of MAX phase synthesis and (b) crystal structure of Ti_3AlC_2 MAX phase.

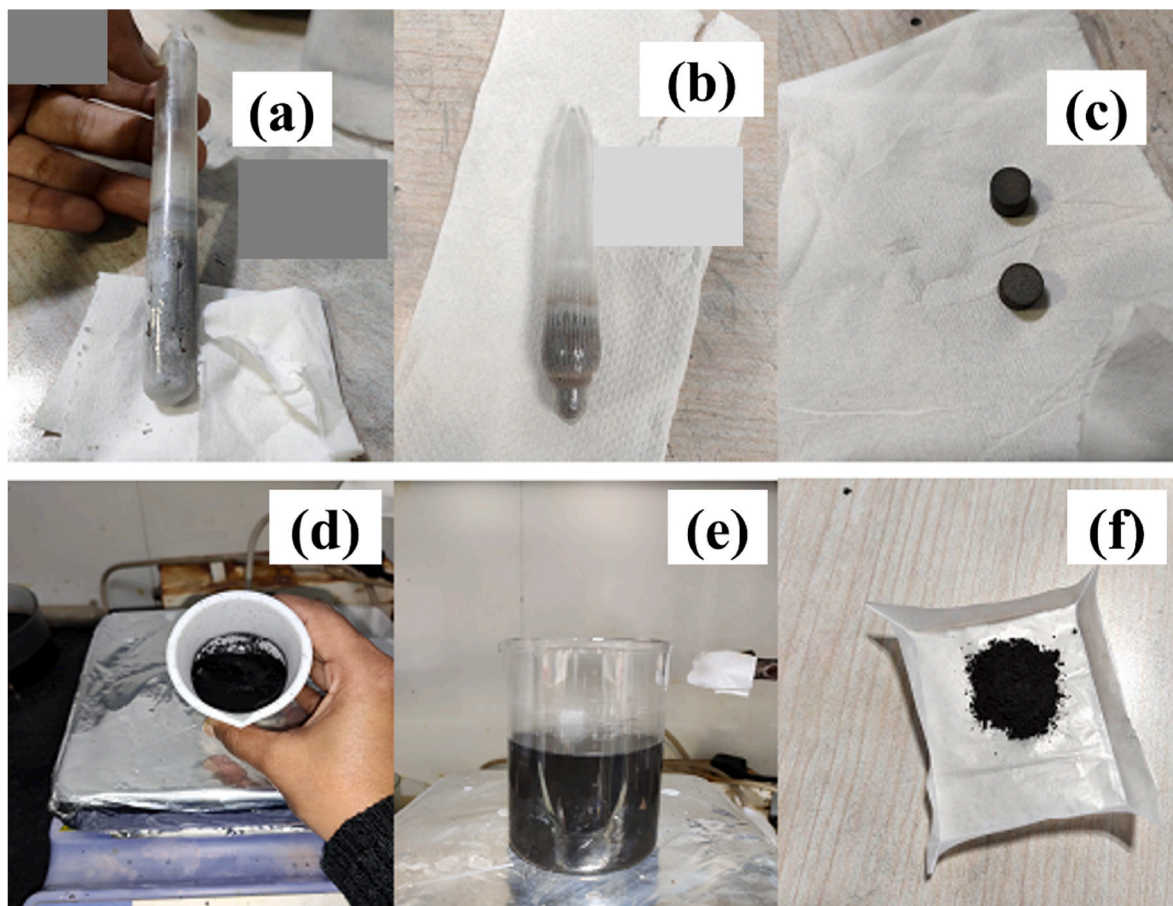


Fig. 2. Quartz ampoule after heat treatment at (a) 1300 °C for 2 h, (b) 1350 °C for 1 hr, (c) samples after thermal treatment, (d) Selective etching of Al from Ti_3AlC_2 phase in 48 wt% HF, (e) $Ti_3C_2T_x$ (MXene) suspension in DI water, (f) final product: MXene($Ti_3C_2T_x$).

Based on the XRD peaks intensity shown in Fig. 4(d), it can be said that desired MAX phase (Ti_3AlC_2) fraction is improved significantly with a reduced fraction of TiC when the sub-stoichiometric ratio of precursors (Ti:Al: TiC:1:1.2:1.8) is used. The composition variation and thermal treatment helped create and order C vacancies, which subsequently facilitated the introduction of Al into the MAX (Ti_3AlC_2) phase. Al goes directly into those vacant sites and forms bonds with TiC. Earlier researchers [24] also observed that it is possible to get Ti_3AlC_2 by intentionally adding C vacant sites into the structure. A. Agresti et al. [25] prepared Ti_3AlC_2 using Ti:Al:TiC:3:1.1:1.9 non-stoichiometric ratio. In the present work, further reducing C vacant sites by lowering TiC precursor content does not provide a better yield of Ti_3AlC_2 . K. J Cai [26] also reported a similar theory.

3.2. Raman spectroscopy

Raman spectrum provides molecular fingerprints and information about the bonds present in the structure by measuring lattice vibrations. Fig. 5(a-b) shows that the Raman spectrum of MAX (Ti_3AlC_2) and MXene ($Ti_3C_2T_x$) are comparable at room temperature when a 532 nm laser is used. Y. Yoon et al. [27] also reported a similar spectrum of MAX and MXene. We observed four prominent peaks in the 100 to 800 cm^{-1} range. In MAX (Ti_3AlC_2), peaks at 126, 226, and 426 cm^{-1} can be assigned to E_{2g} , E_{1g} [28], and A_{1g} vibrational modes [27,28], respectively. The previous report [26] suggests that non-stoichiometric TiC_x is responsible for the former peaks. A peak at 606 cm^{-1} can be assigned to E_{2g} [27] vibrational modes corresponding to the C sub-lattice. E_g , E_{2g} , and A_{1g} modes depict in-plane vibration of Ti, Al, and C bonds [26,27,29]. Peaks at 1375 and 1578 cm^{-1} correspond to D and G bands of

graphitic carbon. In comparing with Raman spectra of MXene, we can say that the etching of Al has not eliminated any of these modes. Some surface functional groups (O, OH, and F) are adsorbed and intercalated within the interlayer spacing. Their distribution affected lattice vibrations of the unit cell, as more atoms vibrated together. These vibrations result in the form of peak shifting and broadening. This data is in good agreement with the broadening of XRD peaks of MXene ($Ti_3C_2T_x$). The peak at 126 cm^{-1} (MAX) is shifted to 122 cm^{-1} (MXene), showing in-plane vibration Ti atoms. The peak at 226 cm^{-1} is shifted to 236 cm^{-1} , which shows the mixed contribution from out-of-plane vibration of the Ti-C bond and H atoms of $Ti_3C_2(OH)_2$ [28]. A peak at 426.7 is softened to 411.8 and corresponds to in-plane vibration of O atoms of OH terminated MXene. A peak at 606 cm^{-1} is also softened to 601 cm^{-1} showing in-plane vibration of the Ti-C bond. As shown in Fig. 5(b), the D band with A_{1g} [26] vibrational mode and the G band with E_{2g} [26] vibrational mode at 1375 cm^{-1} and 1578 cm^{-1} , respectively, are shifted implying out-of-plane vibration of C atoms and unit cell distortion [27, 28]. This way Raman spectrum of MXene ($Ti_3C_2T_x$) shows that Al is selectively removed, but the hexagonal structure of the parent phase is retained and all basic Raman modes are preserved.

3.3. Microstructure analysis

TEM (Transmission Electron Microscopy) and FESEM (Field Emission Scanning Electron Microscopy) are carried out for morphological and microstructural analysis. Fig. 6(a) shows the dense, layered structure of MAX (Ti_3AlC_2), connected by metallic bonding and preferred growth of the crystalline phase in the c direction. Fig. 6(b) shows the presence of kinked laminates, which are responsible for the flexibility of

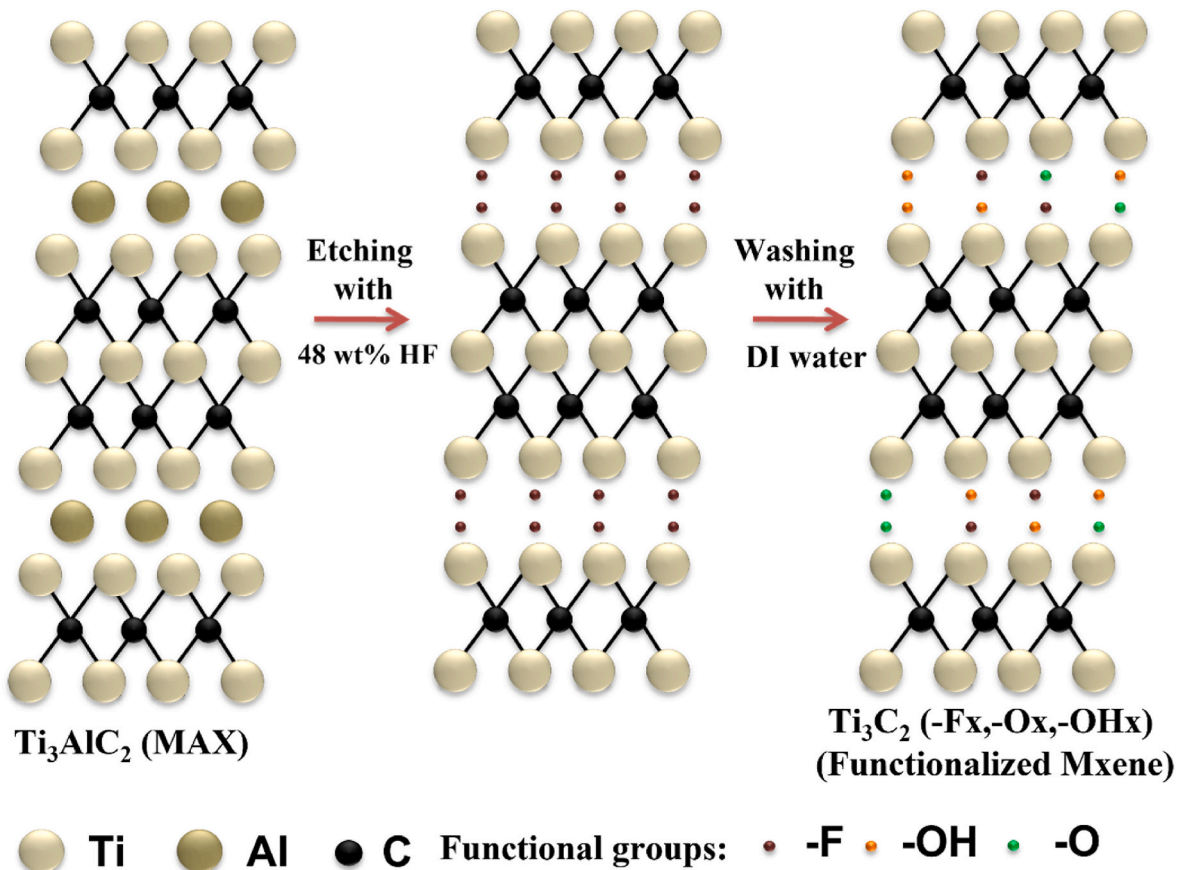


Fig. 3. Schematic of MAX phase and Functionalized MXene.

Ti₃AlC₂. Eduardo et al. [30] reported that these kink bands and the MAX phase nano-laminated structure are accountable for its shock absorption resistance.

Fig. 6(c-d) shows the 2D multilayered structure of MXene (Ti₃C₂T_x). After etching with 48 wt% HF and removal of Al, increased spacing between the layers indicates successive exfoliation of Ti₃AlC₂ and formation of Ti₃C₂T_x (T_x: Functional groups O; OH; F). These results support the peak shifting and broadening of (002) in the XRD pattern of MXene. We found that the accordion-like open layer structure has an average interlayer spacing of ~116 nm, as shown in Fig. 6(d), which is better than that reported by Zhang et al. [31], and an average layer thickness of ~74.4 nm, matching the earlier data [32]. Fig. 6(e) shows the atomic percentage of Ti, Al, and C in the MAX recorded by EDXS. Fig. 6(f) implies the removal of Al atoms and the presence of F, OH, and O functional groups on the surface of MXene sheets. To further verify the structure of MXene, TEM analysis is done. Fig. 7 (a) shows the IFFT (Inverse Fast Fourier Transform) pattern of MXene, which demonstrates the selected area with lattice fringes. These fringes are 0.486 nm apart and agree with the reported values [33]. This inter-lamellar spacing is compared with the 'd' values obtained from XRD data analysis of MXene (Ti₃C₂T_x) and matches the d-spacing of the (004) plane. Fig. 7(b) shows the SAED (Selective Area Electron Diffraction) pattern of the MXene, implying hexagonal symmetry of the structure as reported in the literature [23,34]. We can conclude that Ti₃C₂T_x retained the crystallinity and symmetry of the parent phase Ti₃AlC₂.

3.4. XPS analysis

To characterize the surface chemical composition of the MAX (Ti₃AlC₂) and MXene (Ti₃C₂T_x), X-Ray photoelectron spectroscopy (XPS) analysis is conducted. XPS spectra of MAX (Ti₃AlC₂) confirm the

presence of Ti, C, and Al elements, as shown in Fig. 8. All the binding energies are calibrated with the contingent value of C, i.e., 284.8 eV. Table 1 shows the binding energy and fraction of each component. Al 2p core level peaks, as shown in Fig. 8(a), confirm the presence of metallic Al, Al₂O₃, and Al(OH)₃ peaks, similar to what is reported in the literature [35]. These peaks generally appear due to working in an open lab environment. Fig. 8(b) shows the fitted peaks of C 1s spectra, demonstrating that C is present as Ti-C, C-C, -CO/CH_x, and -COO components. Fitted Ti 2p core-level peaks confirm the presence of Ti as Ti-C in Ti₃AlC₂, as shown in Fig. 8(c).

Fig. 9 depicts the XPS spectra of MXene (Ti₃C₂T_x) and implies that along with Ti and C, some surface functional groups like -O, -OH, and -F are also present in the MXene. After etching, Al is successfully removed from the structure, as shown in Fig. 9(a). Fig. 9(b) depicts fitted peaks of the C 1s core level. We can see that the C1s spectra of MAX and MXene do not offer much difference. Table 1 shows that with the formation of MXene, surface functional groups affected the fraction of Ti-C, C-C, and -CO bonds. Fig. 9(c) plots the fitted peaks of the Ti 2p core level. The presence of functional groups on the surface of MXene improved the bond strength of surface Ti atoms and shifted the peaks towards higher binding energies as evident from Table 1, which also matches with the reported data [36]. After etching, the peak intensity of Ti⁺³ and Ti⁺⁴ is increased as shown in Fig. 9(c), and a report by Li et al. [37] also confirms this finding. The reduced fraction of Ti⁺² shows the oxidation of Ti into Ti⁺³ and Ti⁺⁴ oxidation states and the attachment of -O and -OH atoms to the surface Ti atoms. Fig. 9 (d-e) confirm the presence of -O, -OH, and -F functional groups on the surface of MXene.

3.5. UV-visible spectroscopy

Fig. 10 shows the absorbance behavior of MXene-ethanol solution. A

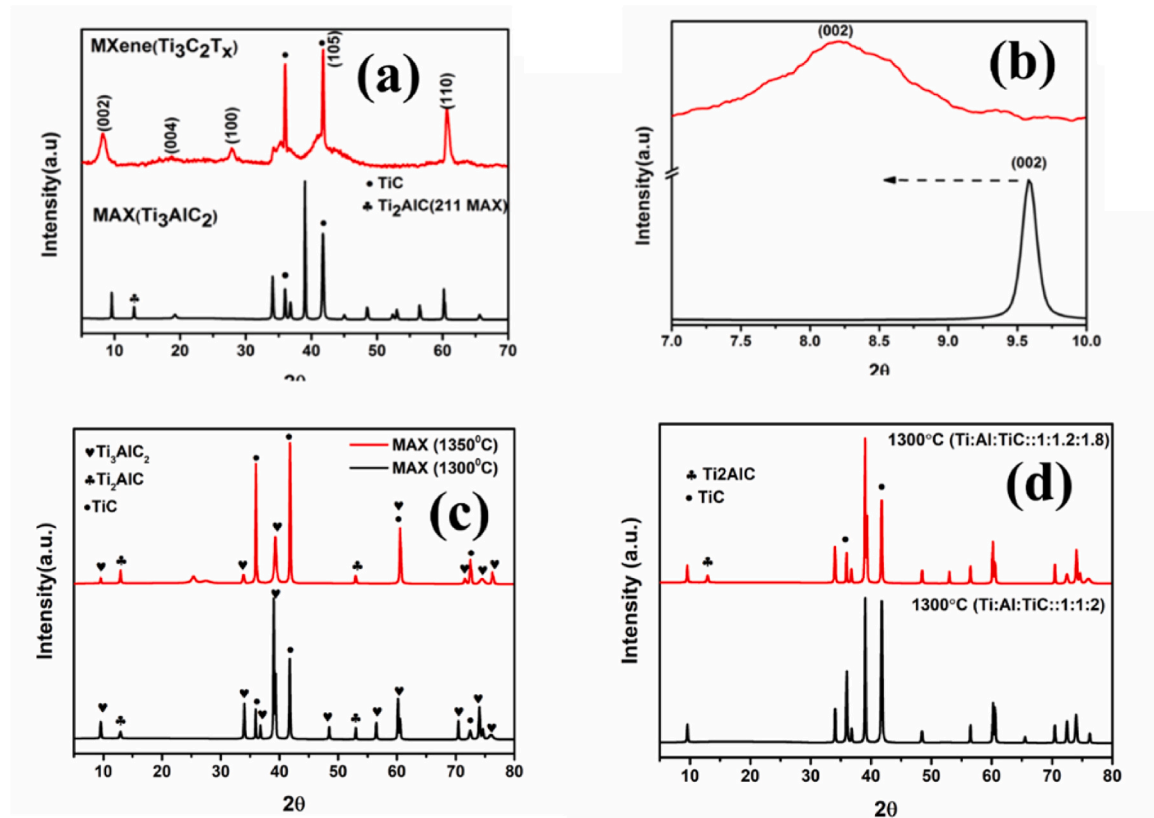


Fig. 4. (a) XRD pattern of the MAX phase and MXene after calcination at 1300°C : precursors are in sub-stoichiometric ratio $\text{Ti:Al:TiC::1:1.2:1.8}$. (b) Shifting of the (002) peak towards a lower 2Θ value shows expansion between the layers of MXene. (c) XRD pattern of samples synthesized at 1300°C and 1350°C shows the decomposition of Ti_3AlC_2 into TiC and Ti_2AlC after calcination at 1350°C . (d) Comparison of XRD pattern of stoichiometric (Ti:Al:TiC::1:1:2) and sub-stoichiometric ($\text{Ti:Al:TiC::1:1:2:1.8}$) compositions synthesized at 1300°C .

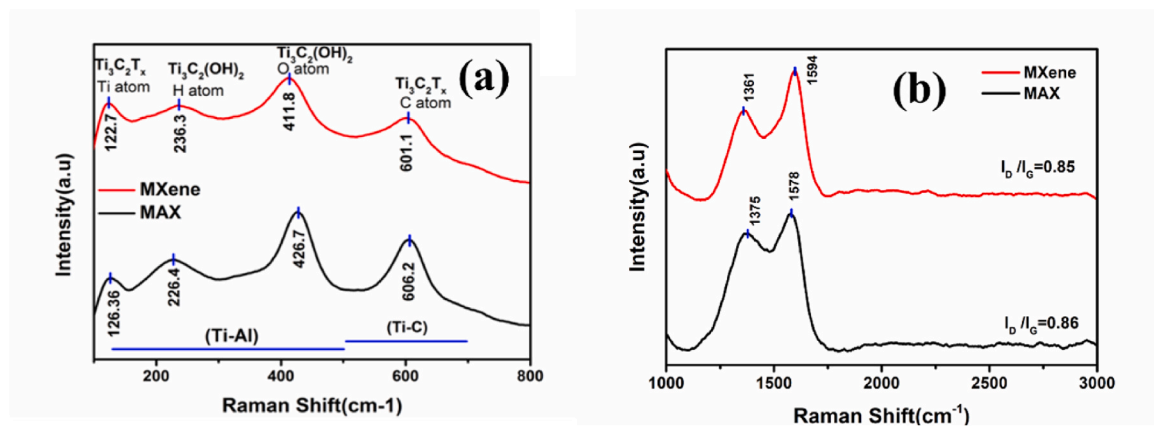


Fig. 5. Raman spectra of (a) MAX (Ti_3AlC_2) and (b) MXene ($\text{Ti}_3\text{C}_2\text{T}_x$; T_x is a functional group).

1mg/3 ml solution was filtered using a $0.22\text{ }\mu\text{m}$ pore size PVDF filter to collect the absorbance data. It is observed that MXene ($<0.22\text{ }\mu\text{m}$) has excellent transmittance in the visible range and shows a broad absorbance peak in the NIR region (815 nm). Absorption peak in the NIR reason also shows LSPR (Localized Surface-Plasmon Resonance) effect as shown in Ref. [42]. These characteristics make MXene a suitable candidate for biosensing applications [43–48], protein detection [49–53], multicolor cellular imaging [54], and photothermal imaging [55]. We obtained an extinction coefficient of $21.2\text{ L g}^{-1}\text{cm}^{-1}$, as shown in Fig. 10(b), which is much better than GO ($7.3\text{ L g}^{-1}\text{cm}^{-1}$) [56] and near the values ($25.67\text{ L g}^{-1}\text{cm}^{-1}$) reported by Lin p et al. [57].

3.6. I-V characteristic

Fig. 11(a) shows the linear I-V curve, which verifies the metallic behavior of the MXene sample. To further confirm the metallic nature of the sample, band structure calculation was done by density functional theory (DFT) analysis using quantum espresso, and Fig. 11(b) shows the zero-band gap of the MAX phase. The electronic conductivity of the cold-pressed MXene pellet (0.1 mm thickness) is measured by the four-probe van der Pauw method at room temperature. We obtained $\sim 2556\text{ S/m}$ of conductivity, which is in good accordance with the literature [58]. The cold-pressed thin pellet has high resistance due to functional defects and high inter-flake resistance. Cold pressing with 2 kN pressure does not

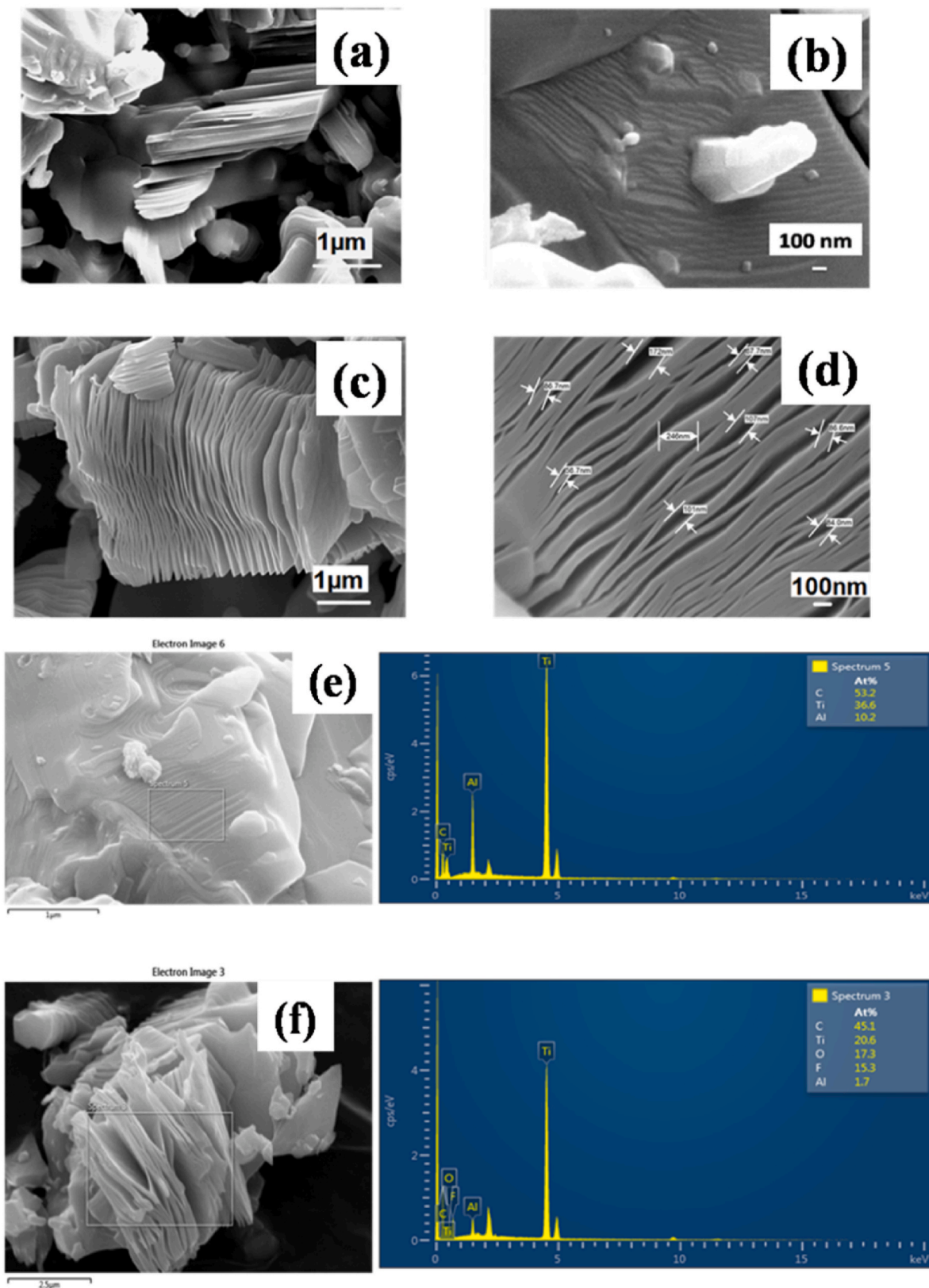


Fig. 6. FESEM images of (a) MAX (Ti_3AlC_2) (b) formation of kink bands on the surface of MAX phase. (c) MXene ($Ti_3C_2T_x$) (d) An open layer structure of MXene with an average interlayer spacing of 116 nm. EDS (Energy Dispersive Spectroscopy) data of (e) MAX and (f) MXene.

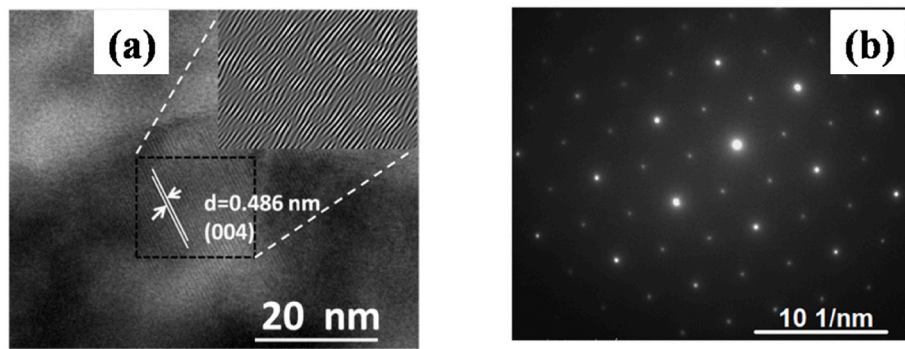


Fig. 7. TEM images of MXene (a) IFFT pattern show d-spacing of (004), which is well-matched with the data obtained from XRD. (b) SAED pattern confirms the hexagonal crystal structure of MXene.

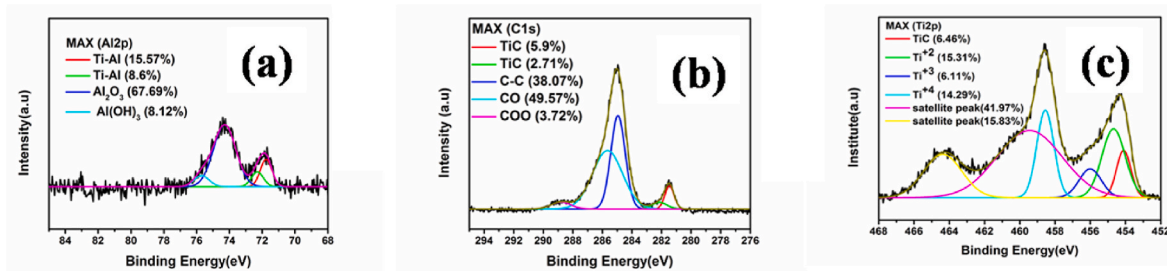


Fig. 8. Fitted peaks of (a) Al 2p, (b) C 1s, and (c) Ti 2p core levels of the MAX phase.

Table 1

Ti₃AlC₂ and Ti₃C₂T_x XPS peak fitting result: Parameters like peak position and percentage of the components are obtained by peak fitting XPS spectra by Gaussian-Lorentzian curve.

Phase	Region	Component	Binding energy (eV)	Percentage (%)	This work &Ref.
Ti ₃ AlC ₂ (MAX)	Ti 2p 3/2 (14.52 at%)	Ti-C	454.1	6.46	[35,38]
		Ti ⁺²	454.75	15.31	[36,39]
		Ti ⁺³	455.78	6.11	[36,39]
		Ti ⁺⁴	458.54	14.29	[35,36]
	Ti 2p 1/2	Satellite peak	459.54 464.35	41.97 15.83	[40]
	Al 2p 3/2; 2p 1/2 (12.22 at%)	Ti-Al	71.6 (72.2)	15.57 (8.6)	[35]
		Al ₂ O ₃	74.29	67.69	[35]
		Al(OH) ₃	75.63	8.12	[41]
	C(1s) (73.25 at%)	Ti-C	281.48	5.9	[34,35,37]
		Ti-C	282.25	2.71	[34]
Ti ₃ C ₂ T _x (MXene)	C(1s) (53.91 at%)	C-C	284.96	38.07	[35]
		-CO/CH _x	286.11	49.57	[35]
		-COO	288.79	3.72	[35]
	Ti 2p 3/2 (13.75 at%)	Ti-C-T _x	454.47	5.06	[38]
		Ti ⁺²	455.35	10.12	[38]
		Ti ⁺³	456.59	9.17	[38]
		Ti ⁺⁴	459.06	27.54	[38]
	Ti 2p 1//2	Satellite peak	460.29 464.91	32.01 16.07	
	Al 2p 3/2; 2p 1/2 (1.9 at%)	—	—	—	—
	C(1s) (22.26 at%)	Ti-C-T _x	281.46	2.15	[35,38]
		Ti-C-T _x	282.38	3.99	[34,37,38]
		C-C	284.81	45.69	[34,35,37,38]
		-CO/CH _x	286.23	43.2	[34,35,38]
		-COO	288.54	4.91	[34,35,38]
	O(1s) (8.16 at%)	Ti-C-O _x	530.07	30.55	[38]
		Ti-C-OH _x	531.69	69.42	[38]
	F(1s) (8.16 at%)	Ti-C-F _x	684.66	87.78	[38]
		Al-F	685.83	12.22	[38]

provide a highly dense pellet, as only 57% of the theoretical density (4.07g/cc) [59] was achieved. Hence, we have found higher resistivity.

4. Conclusion

We prepared the Ti₃AlC₂ (MAX) phase and its derived Ti₃C₂T_x (MXene) using a single-step synthesis route. Further, we have shown

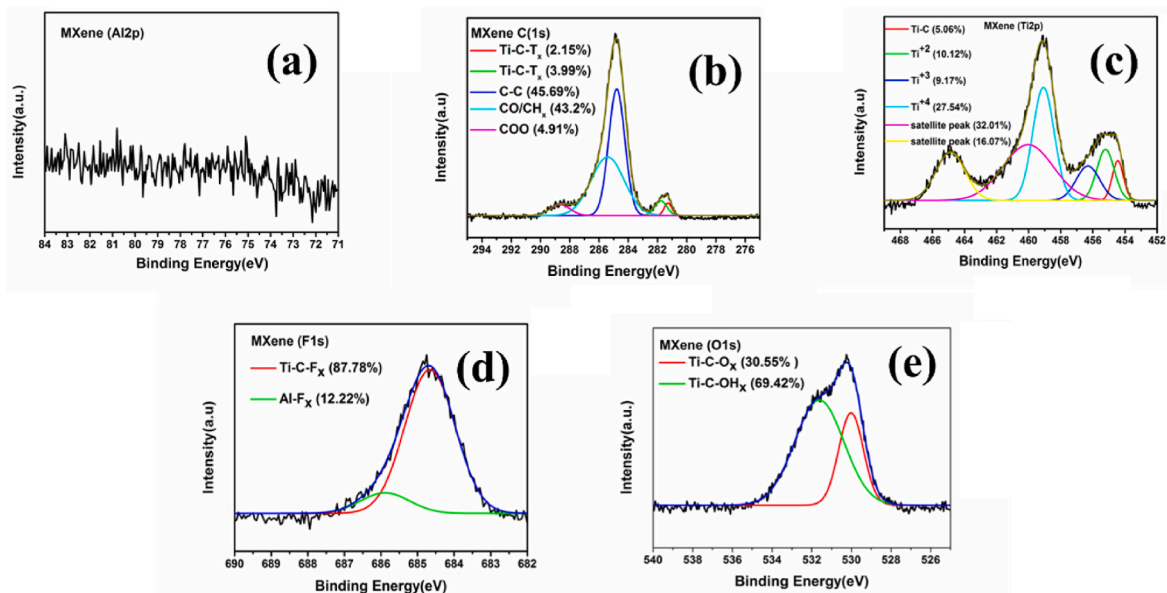


Fig. 9. Fitted peaks of (a) Al 2p, (b) C 1s, (c) Ti 2p, (d) F 1s, and (f) O 1s core levels of MXene.

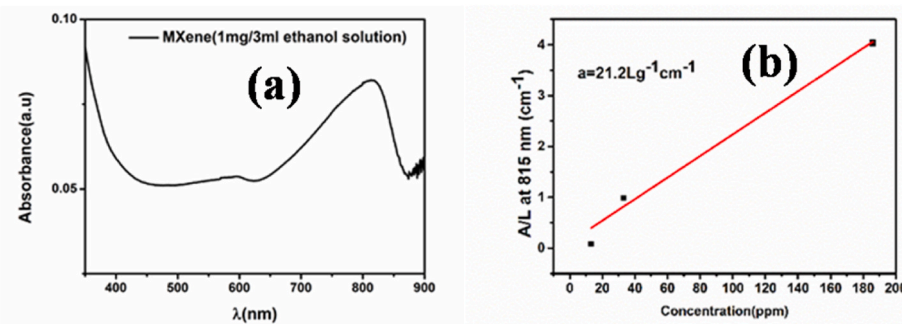


Fig. 10. UV-Visible spectra (a) absorbance vs. wavelength graph of MXene (<0.22 μm) solution showing broad absorbance peak in the NIR region. (b) Absorbance path length vs. concentration graph: the slope of the graph shows the extinction coefficient of the MXene dispersed in ethanol.

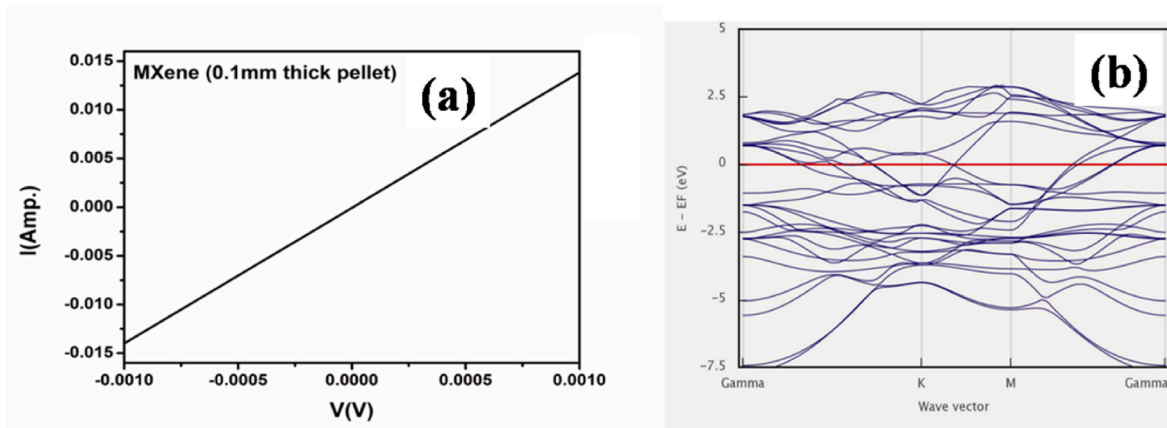


Fig. 11. (a) I-V characteristic of 0.1 mm thick MXene pellet. (b) The band structure of the MAX phase obtained from the DFT calculation shows a “Zero” bandgap.

that a sub-stoichiometric amount of TiC precursor produces a better yield in the fraction of the Ti_3AlC_2 MAX phase. Having precise control over the precursor's composition and reaction kinetics makes it possible further to reduce the TiC fraction in the final product. XRD peaks confirm that the interplanar spacing increases after etching the MAX phase with HF. Raman spectroscopy and SAED pattern ensure that the

removal of Al didn't distort the original hexagonal structure of the MAX phase. XPS and Raman peaks show surface functional groups (-O, -OH, and -F) on the MXene surface. The hexagonal structure of MXene and the presence of D, and G bands with $I_D/I_G < 1$ confirm that MXene is analogous to graphene with high electrical conductivity because of the ordered crystal structure. The absence of the right set of resources often

restricts to work on new generation materials. No use of milling media or an expensive tool like a hot press; small dwelling time, and the right set of precursors make this process less time-consuming. This single-step processing technique can also be adopted for producing various MAX phase compositions.

Declaration of competing interest

The authors declare that they have no known competing financial interests or personal relationships that could have appeared to influence the work reported in this paper.

Acknowledgment

This work is supported by a grant from Science and Engineering Research Board, DST (SERB-DST), India (Grant No: IMP/2018/000955).

References

- [1] M. Alhabeb, K. Maleski, B. Anasori, P. Lelyukh, L. Clark, S. Sin, Y. Gogotsi, Guidelines for synthesis and processing of two-dimensional titanium carbide (Ti3C2Tx MXene), *Chem. Mater.* 29 (2017) 7633–7644.
- [2] G.S. Gund, J.H. Park, R. Harpal Singh, M. Kota, J.H. Shin, T. Kim, Y. Gogotsi, H. S. Park, MXene/polymer hybrid materials for flexible AC-filtering electrochemical capacitors, *Joule* 3 (2019) 164–176.
- [3] O. Mashtalir, M. Naguib, V.N. Mochalin, Y. Dall'Agne, M. Heon, M.W. Barsoum, Y. Gogotsi, Intercalation and delamination of layered carbides and carbonitrides, *Nat. Commun.* 4 (2013) 1–7.
- [4] A. Lipatov, H. Lu, M. Alhabeb, B. Anasori, A. Gruverman, Y. Gogotsi, A. Sinitskii, Elastic properties of 2D Ti3C2Tx MXene monolayers and bilayers, *Sci. Adv.* 4 (2018), eaat0491.
- [5] A.S. Zeraati, S.A. Mirkhani, P. Sun, M. Naguib, P. V. Braun, U. Sundararaj, Improved synthesis of Ti 3 C 2 T x MXenes resulting in exceptional electrical conductivity, high synthesis yield, and enhanced capacitance, *Nanoscale* 13 (2021) 3572–3580.
- [6] A. Morales-Garcia, F. Calle-Vallejo, F. Illas, MXenes: new horizons in catalysis, *ACS Catal.* 10 (2020) 13487–13503.
- [7] F. Dixit, K. Zimmermann, R. Dutta, N.J. Prakash, B. Barbeau, M. Mohseni, B. Kandasubramanian, Application of MXenes for water treatment and energy-efficient desalination: a review,, *J. Hazard Mater.* 423 (2022), 127050.
- [8] J. Ran, G. Gao, F.-T. Li, T.-Y. Ma, A. Du, S.-Z. Qiao, Ti 3 C 2 MXene co-catalyst on metal sulfide photo-absorbers for enhanced visible-light photocatalytic hydrogen production, *Nat. Commun.* Now. 8 (2017) 1–10.
- [9] S.J. Kim, H.-J. Koh, C.E. Ren, O. Kwon, K. Maleski, S.-Y. Cho, B. Anasori, C.-K. Kim, Y.-K. Choi, J. Kim, Metallic Ti3C2Tx MXene gas sensors with ultrahigh signal-to-noise ratio, *ACS Nano* 12 (2018) 986–993.
- [10] J. Liu, H. Zhang, R. Sun, Y. Liu, Z. Liu, A. Zhou, Z. Yu, Hydrophobic, flexible, and lightweight MXene foams for high-performance electromagnetic-interference shielding, *Adv. Mater.* 29 (2017), 1702367.
- [11] S. Xu, G. Wei, J. Li, Y. Ji, N. Klyui, V. Izotov, W. Han, Binder-free Ti3C2Tx MXene electrode film for supercapacitor produced by electrophoretic deposition method, *Chem. Eng. J.* 317 (2017) 1026–1036.
- [12] D. Xiong, X. Li, Z. Bai, S. Lu, Recent advances in layered Ti3C2Tx MXene for electrochemical energy storage, *Small* 14 (2018), 1703419.
- [13] B. Anasori, M.R. Lukatskaya, Y. Gogotsi, 2D metal carbides and nitrides (MXenes) for energy storage, *Nat. Rev. Mater.* 2 (2017) 1–17.
- [14] C.H. Michel W. Barsoum, Nanolaminated 2-2-1 MAX-phase Compositions, US10538431B2, n.d.
- [15] T.S. Chngfeng Hu, Salvatore Grasso, Yoshio Sakka, Hidehiko Tanaka, Max-phase Oriented Ceramic and Method for Producing the Same, US20130052438, n.d.
- [16] T. Goto, T. Hirai, Chemically vapor deposited Ti3SiC2, *Mater. Res. Bull.* 22 (1987) 1195–1201.
- [17] R. Pampuch, J. Lis, L. Stobierski, M. Tymkiewicz, Solid combustion synthesis of Ti3SiC2, *J. Eur. Ceram. Soc.* 5 (1989) 283–287.
- [18] C. Racault, F. Langlais, R. Naslain, Solid-state synthesis and characterization of the ternary phase Ti 3 SiC 2, *J. Mater. Sci.* 29 (1994) 3384–3392.
- [19] J.E. von Treifeldt, K.L. Firestein, J.F.S. Fernando, C. Zhang, D.P. Siriwardena, C.-E. M. Lewis, D. V Goldberg, The effect of Ti3AlC2 MAX phase synthetic history on the structure and electrochemical properties of resultant Ti3C2 MXenes, *Mater. DES* 199 (2021), 109403.
- [20] C.E. Shuck, M. Han, K. Maleski, K. Hantanasirisakul, S.J. Kim, J. Choi, W.E.B. Reil, Y. Gogotsi, Effect of Ti3AlC2 MAX phase on structure and properties of resultant Ti3C2Tx MXene, *ACS Appl. Nano Mater.* 2 (2019) 3368–3376.
- [21] F. Kong, X. He, Q. Liu, X. Qi, Y. Zheng, R. Wang, Y. Bai, Effect of Ti3AlC2 precursor on the electrochemical properties of the resulting MXene Ti3C2 for Li-ion batteries, *Ceram. Int.* 44 (2018) 11591–11596.
- [22] X. Lu, Y. Zhou, Pressureless sintering and properties of Ti3AlC2, *Int. J. Appl. Ceram. Technol.* 7 (2010) 744–751.
- [23] P. Nayak, Q. Jiang, R. Mohanraman, D. Anjum, M.N. Hedhili, H.N. Alshareef, Inherent electrochemistry and charge transfer properties of few-layered two-dimensional Ti 3 C 2 T x MXene, *Nanoscale* 10 (2018) 17030–17037.
- [24] D.P. Riley, E.H. Kisi, The design of crystalline precursors for the synthesis of Mn–1AXn phases and their application to Ti3AlC2, *J. Am. Ceram. Soc.* 90 (2007) 2231–2235.
- [25] A. Agresti, A. Pazniak, S. Pescetelli, A. Di Vito, D. Rossi, A. Pecchia, M.A. der Maur, A. Liedl, R. Larciprete, D. V Kuznetsov, Titanium-carbide MXenes for work function and interface engineering in perovskite solar cells, *Nat. Mater.* 18 (2019) 1228–1234.
- [26] K.J. Cai, Y. Zheng, P. Shen, S.Y. Chen, TiC x-Ti 2 C nanocrystals and epitaxial graphene-based lamellae by pulsed laser ablation of bulk TiC in vacuum, *CrystEngComm* 16 (2014) 5466–5474.
- [27] Y. Yoon, T.A. Le, A.P. Tiwari, I. Kim, M.W. Barsoum, H. Lee, Low temperature solution synthesis of reduced two dimensional Ti 3 C 2 MXenes with paramagnetic behaviour, *Nanoscale* 10 (2018) 22429–22438.
- [28] A. Sarycheva, Y. Gogotsi, Raman spectroscopy analysis of the structure and surface chemistry of Ti3C2Tx MXene, *Chem. Mater.* 32 (2020) 3480–3488.
- [29] M. Naguib, M. Kurtoglu, V. Presser, J. Lu, J. Niu, M. Heon, L. Hultman, Y. Gogotsi, M.W. Barsoum, Two-dimensional nanocrystals produced by exfoliation of Ti3AlC2, *Adv. Mater.* 23 (2011) 4248–4253.
- [30] E. Tabares, A. Jiménez-Morales, S.A. Tsipas, Study of the synthesis of MAX phase Ti3SiC2 powders by pressureless sintering, *Boletín La Soc. Española Cerámica y Vidr* 60 (2021) 41–52.
- [31] F. Zhang, Y. Zhou, Y. Zhang, D. Li, Z. Huang, Facile synthesis of sulfur@ titanium carbide MXene as high performance cathode for lithium-sulfur batteries, *Nanophotonics* 9 (2020) 2025–2032.
- [32] N.K. Chaudhari, H. Jin, B. Kim, D. San Baek, S.H. Joo, K. Lee, MXene: an emerging two-dimensional material for future energy conversion and storage applications, *J. Mater. Chem. 5* (2017) 24564–24579.
- [33] Y. Lei, N. Tan, Y. Zhu, D. Huo, S. Sun, Y. Zhang, G. Gao, Synthesis of porous N-rich carbon/MXene from MXene@ polypyrrole hybrid nanosheets as oxygen reduction reaction electrocatalysts, *J. Electrochim. Soc.* 167 (2020), 116503.
- [34] B. Ahmed, D.H. Anjum, M.N. Hedhili, Y. Gogotsi, H.N. Alshareef, H 2 O 2 assisted room temperature oxidation of Ti 2 C MXene for Li-ion battery anodes, *Nanoscale* 8 (2016) 7580–7587.
- [35] L.-Å. Naslund, P.O.Å. Persson, J. Rosen, X-Ray photoelectron spectroscopy of Ti3AlC2, Ti3C2Tx, and TiC provides evidence for the electrostatic interaction between laminated layers in MAX-phase materials, *J. Phys. Chem. C* 124 (2020) 27732–27742.
- [36] J. Halim, M.R. Lukatskaya, K.M. Cook, J. Lu, C.R. Smith, L.-Å. Naslund, S.J. May, L. Hultman, Y. Gogotsi, P. Eklund, Transparent conductive two-dimensional titanium carbide epitaxial thin films, *Chem. Mater.* 26 (2014) 2374–2381.
- [37] J. Li, R. Qin, L. Yan, Z. Chi, Z. Yu, H. Chen, G. Shan, M. Hu, Plasmonic Light Illumination Creates a Channel to Achieve Fast Degradation of Ti 3 C 2 Tx Nanosheets, (n.d.).
- [38] S.A. Shah, T. Habib, H. Gao, P. Gao, W. Sun, M.J. Green, M. Radovic, Template-free 3D titanium carbide (Ti 3 C 2 T x) MXene particles crumpled by capillary forces, *Chem. Commun.* 53 (2017) 400–403.
- [39] A. Biswas, A. Sengupta, U. Rajput, S.K. Singh, V. Antad, S.M. Hossain, S. Parmar, D. Rout, A. Deshpande, S. Nair, Growth, properties, and applications of pulsed laser deposited nanolaminate Ti 3 Al C 2 thin films, *Phys. Rev. Appl.* 13 (2020), 44075.
- [40] G. Greczynski, J. Jensen, J.E. Greene, I. Petrov, L. Hultman, X-ray photoelectron spectroscopy analyses of the electronic structure of polycrystalline Ti1-xAlxN thin films with 0≤x≤0.96, *Surf. Sci. Spectra* 21 (2014) 35–49.
- [41] A. Barrera, F. Tzompantzi, J. Campa-Molina, J.E. Casillas, R. Pérez-Hernández, S. Ulloa-Godínez, C. Velasquez, J. Arenas-Alatorre, Photocatalytic activity of Ag/Al 2 O 3 -Gd 2 O 3 photocatalysts prepared by the sol-gel method in the degradation of 4-chlorophenol, *RSC Adv.* 8 (2018) 3108–3119.
- [42] H. Lin, X. Wang, L. Yu, Y. Chen, J. Shi, Two-dimensional ultrathin MXene ceramic nanosheets for photothermal conversion, *Nano Lett.* 17 (2017) 384–391.
- [43] L. Wu, X. Lu, Z.-S. Wu, Y. Dong, X. Wang, S. Zheng, J. Chen, 2D transition metal carbide MXene as a robust biosensing platform for enzyme immobilization and ultrasensitive detection of phenol, *Biosens. Bioelectron.* 107 (2018) 69–75.
- [44] M. Zhu, R. Wang, C. Chen, H.B. Zhang, G.J. Zhang, Comparison of corrosion behavior of Ti 3 SiC 2 and Ti 3 AlC 2 in NaCl solutions with Ti, *Ceram. Bar Int.* 43 (2017) 5708–5714, <https://doi.org/10.1016/j.ceramint.2017.01.111>.
- [45] F. Wang, C. Yang, M. Duan, Y. Tang, J. Zhu, TiO2 nanoparticle modified organ-like Ti3C2 MXene nanocomposite encapsulating hemoglobin for a mediator-free biosensor with excellent performances, *Biosens. Bioelectron.* 74 (2015) 1022–1028.
- [46] R.B. Rakhi, P. Nayak, C. Xia, H.N. Alshareef, Novel amperometric glucose biosensor based on MXene nanocomposite, *Sci. Rep.* 6 (2016) 1–10.
- [47] H. Liu, C. Duan, C. Yang, W. Shen, F. Wang, Z. Zhu, A novel nitrite biosensor based on the direct electrochemistry of hemoglobin immobilized on MXene-Ti3C2, *Sensor. Actuator. B Chem.* 218 (2015) 60–66.
- [48] M. Wu, Q. Zhang, Y. Fang, C. Deng, F. Zhou, Y. Zhang, X. Wang, Y. Tang, Y. Wang, Polylysine-modified MXene nanosheets with highly loaded glucose oxidase as cascade nanoreactor for glucose decomposition and electrochemical sensing, *J. Colloid Interface Sci.* 586 (2021) 20–29.
- [49] A. Zamhuri, G.P. Lim, N.L. Ma, K.S. Tee, C.F. Soon, MXene in the lens of biomedical engineering: synthesis, applications and future outlook, *Biomed. Eng. Online* 20 (2021) 1–24.
- [50] Q. Xu, L. Ding, Y. Wen, W. Yang, H. Zhou, X. Chen, J. Street, A. Zhou, W.-J. Ong, N. Li, High photoluminescence quantum yield of 18.7% by using nitrogen-doped Ti 3 C 2 MXene quantum dots, *J. Mater. Chem. C* 6 (2018) 6360–6369.
- [51] Z. Guo, X. Zhu, S. Wang, C. Lei, Y. Huang, Z. Nie, S. Yao, Fluorescent Ti 3 C 2 MXene quantum dots for an alkaline phosphatase assay and embryonic stem cell identification based on the inner filter effect, *Nanoscale* 10 (2018) 19579–19585.

- [52] G. Cai, Z. Yu, P. Tong, D. Tang, Ti 3 C 2 MXene quantum dot-encapsulated liposomes for photothermal immunoassays using a portable near-infrared imaging camera on a smartphone, *Nanoscale* 11 (2019) 15659–15667.
- [53] Q. Zhang, Y. Sun, M. Liu, Y. Liu, Selective detection of Fe 3+ ions based on fluorescence MXene quantum dots via a mechanism integrating electron transfer and inner filter effect, *Nanoscale* 12 (2020) 1826–1832.
- [54] Q. Xue, H. Zhang, M. Zhu, Z. Pei, H. Li, Z. Wang, Y. Huang, Y. Huang, Q. Deng, J. Zhou, Photoluminescent Ti3C2 MXene quantum dots for multicolor cellular imaging, *Adv. Mater.* 29 (2017), 1604847.
- [55] Z. Huang, X. Cui, S. Li, J. Wei, P. Li, Y. Wang, C.-S. Lee, Two-dimensional MXene-based materials for photothermal therapy, *Nanophotonics* 9 (2020) 2233–2249.
- [56] M. Ojrzyńska, A. Wroblewska, J. Judek, A. Malolepszy, A. Dużynska, M. Zdrojek, Study of optical properties of graphene flakes and its derivatives in aqueous solutions, *Opt Express* 28 (2020) 7274–7281.
- [57] P. Lin, J. Xie, Y. He, X. Lu, W. Li, J. Fang, S. Yan, L. Zhang, X. Sheng, Y. Chen, MXene aerogel-based phase change materials toward solar energy conversion, *Sol. Energy Mater. Sol. Cells* 206 (2020), 110229.
- [58] M. Naguib, O. Mashtalir, J. Carle, V. Presser, J. Lu, L. Hultman, Y. Gogotsi, M. W. Barsoum, Two-dimensional transition metal carbides, *ACS Nano* 6 (2012) 1322–1331.
- [59] A.M. Navarro-Suárez, K.L. Van Aken, T. Mathis, T. Makaryan, J. Yan, J. Carretero-González, T. Rojo, Y. Gogotsi, Development of asymmetric supercapacitors with titanium carbide-reduced graphene oxide couples as electrodes, *Electrochim. Acta* 259 (2018) 752–761, <https://doi.org/10.1016/j.electacta.2017.10.125>.